CELL BIOLOGY

Injury-mediated stiffening persistently activates muscle stem cells through YAP and TAZ mechanotransduction

Jason S. Silver[1,2,3,4], K. Arda Günay[1,2], Alicia A. Cutler[3], Thomas O. Vogler[3,4], Tobin E. Brown[1,2], Bradley T. Pawlikowski[3], Olivia J. Bednarski[1,2], Kendra L. Bannister[1,2], Cameron J. Rogowski[1,2], Austin G. Mckay[1,2], Frank W. DelRio[5], Bradley B. Olwin[2,3]*, Kristi S. Anseth[1,2]*

The skeletal muscle microenvironment transiently remodels and stiffens after exercise and injury, as muscle ages, and in myopathic muscle; however, how these changes in stiffness affect resident muscle stem cells (MuSCs) remains understudied. Following muscle injury, muscle stiffness remained elevated after morphological regeneration was complete, accompanied by activated and proliferative MuSCs. To isolate the role of stiffness on MuSC behavior and determine the underlying mechanotransduction pathways, we cultured MuSCs on strain-promoted azide-alkyne cycloaddition hydrogels capable of in situ stiffening by secondary photocrosslinking of excess cyclooctynes. Using pre- to post-injury stiffness hydrogels, we found that elevated stiffness enhances migration and MuSC proliferation by localizing yes-associated protein 1 (YAP) and WW domain–containing transcription regulator 1 (WWTR1; TAZ) to the nucleus. Ablating YAP and TAZ in vivo promotes MuSC quiescence in postinjury muscle and prevents myofiber hypertrophy, demonstrating that persistent exposure to elevated stiffness activates mechanotransduction signaling maintaining activated and proliferating MuSCs.

INTRODUCTION

Skeletal muscle fibers (myofibers) require physical support to function and accommodate stresses generated during muscle contraction and relaxation (*1*). Each myofiber is surrounded by and directly linked to an extracellular matrix (ECM) with an inherent elastic modulus (or stiffness) arising from the presence of cross-linked proteins including collagen, laminin, and fibronectin (*2*). The ECM provides a mechanical base for the myofiber membrane and functions as scaffolding for muscle repair (*3*). While often considered a passive reinforcing structure, the ECM actively participates in physical and biochemical signaling to regulate resident skeletal muscle stem cell (MuSC) orientation, expansion, and differentiation, all critical to maintain and regenerate muscle (*4*). The ECM undergoes transient remodeling during muscle repair, increasing mechanical stiffness with exercise, injury, aging, and myopathies on variable time scales from hours to years (*5*, *6*). Whether elevated stiffness alters muscle function directly and changing MuSC behavior is not known. To investigate the mechanisms regulating MuSCs responses to muscle stiffening, in the absence of other confounding factors, we designed and implemented unique mechanically controlled material microenvironments.

Hydrogels (or biomaterial scaffolds) are tunable, well-defined in vitro environments used to assess the effects of physical stiffness on MuSC function (*7*–*10*). Hydrogels preserve MuSC quiescence ex vivo (*9*), enhance myogenic differentiation (*11*), and promote engraftment into the muscle niche (*8*, *12*). This prior published work is foundational and demonstrates the value of hydrogel scaffolds with tailorable but static mechanical properties (*13*). Building from these studies, we designed hydrogels that recapitulate some of the dynamic changes that occur in ECM mechanics in vivo. We can assess the temporal responses of MuSCs to changes in matrix mechanics by synthesizing a hydrogel where its cross-linking density, hence the physical stiffness, is increased on demand. A bioclick hydrogel with muscle-like stiffness was developed using a strain-promoted azide-alkyne cycloaddition (SPAAC) reaction using poly(ethylene glycol) (PEG) precursors functionalized with dibenzocyclooctyne (DBCO) and azide (N_3) groups (*14*). The cytocompatible SPAAC reaction proceeds rapidly (i.e., ~5 min) at physiological conditions and is bioorthogonal; therefore, it is an attractive platform for both two-dimensional (2D) and 3D cell culture (*15*, *16*). Furthermore, we found that hydrogel formulations containing excess DBCO groups can rapidly photocrosslink, resulting in an in situ stiffening of the hydrogel (*14*). Other dual-cure strategies exist for hydrogel networks in cell culture applications (*17*, *18*), including thiol-Michael additions followed by (meth)acrylate radical polymerization (*19*–*21*). However, our rapid and bioorthogonal cycloaddition provides some benefits over the base-catalyzed conjugate addition for cellular encapsulation and is less prone to network nonidealities, such as disulfide formation (*22*). This light-mediated cross-linking strategy allows spatiotemporal control over the hydrogel properties compared to other bioclick chemistries (*23*, *24*). Thus, photostiffening SPAAC networks are an attractive strategy to understand whether stiffness directly affects MuSC behavior and to elucidate the underlying mechanotransduction pathways involved.

Here, we identify that postinjury stiffening of muscle leads to persistent MuSC proliferation and prevents quiescence acquisition after muscle repair. Using our stiffening SPAAC hydrogels as an in vitro model of the muscle microenvironment, hydrogel stiffening induces proliferative and migratory changes in MuSCs that are mediated by mechanotransduction signaling, which is further supported by in vivo observations.

[1]Department of Chemical and Biological Engineering, University of Colorado, Boulder, CO, USA. [2]BioFrontiers Institute, University of Colorado, Boulder, CO, USA. [3]Department of Molecular, Cellular and Developmental Biology, University of Colorado, Boulder, CO, USA. [4]Medical Scientist Training Program, University of Colorado Anschutz Medical Campus, Aurora, CO, USA. [5]Applied Chemicals and Materials Division, Material Measurement Laboratory, National Institute of Standards and Technology, Boulder, CO, USA.
*Corresponding author. Email: kristi.anseth@colorado.edu (K.S.A.); olwin@colorado.edu (B.B.O.)

RESULTS

Chemical injury increases muscle stiffness and persistently activates MuSCs

In uninjured skeletal muscle, most MuSCs are quiescent with a small number participating in skeletal muscle homeostasis (*25*, *26*).

In regenerated skeletal muscle, MuSCs are similarly assumed to be quiescent. We injured the tibialis anterior (TA) muscle with barium chloride ($BaCl_2$) and asked whether MuSCs in regenerating skeletal muscle at 14 and 28 days after injury reacquired quiescence similar to those in uninjured muscle. Pax7 (paired box 7) protein, but not MyoD (myogenic differentiation 1) protein, is detected in quiescent MuSCs. MyoD identifies activated MuSCs that have exited quiescence, entered S phase, and are committed to proliferation (*27*). A twofold increase in immunoreactive $MyoD^+$ MuSCs was observed at 14 days (37%) and 28 days after injury (39%) on regenerated extensor digitorum longus (EDL) myofibers compared to MuSCs from uninjured contralateral EDL myofibers (18%) (Fig. 1, A and B). To determine the numbers of dividing MuSCs in uninjured and regenerating skeletal muscle, we supplemented a 24-hour pulse of 5-ethynyl-2′-deoxyuridine (EdU) before muscle isolation at 14 and 28 days after injury for injured and uninjured muscle (Fig. 1C). At 28 days after injury, in regenerated muscle compared to uninjured muscle, the numbers of $MyoD^+$ MuSCs (Fig. 1B) and the number of $Pax7^+$ cells per unit areas are twofold greater (Fig. 1D); some MuSCs remain proliferating (Fig. 1E). While MuSCs rapidly activate and proliferate directly after injury, at 28 days after injury, MuSCs have not returned to their default quiescent state and remain activated with a subset persistently undergoing division.

We asked whether muscle stiffness changes following a muscle injury by measuring the elastic modulus (Young's modulus, E') via atomic force microscopy (AFM) at different times after $BaCl_2$ injury of the TA muscle (Fig. 1F). Five days after injury, muscle elasticity decreased by twofold (5 kPa) (Fig. 1, G and H). Subsequently, as regeneration progresses, muscle stiffness rebounds to a Young's modulus that is twofold greater than uninjured muscle by 14 days after injury (19.3 kPa) and persists at least 28 days after injury (22.1 kPa). Since an increase in muscle stiffness is likely accompanied by changes in ECM deposition, we asked whether ECM deposition was increased in regenerated skeletal muscle (Fig. 1I). Collagen deposition is present in the endomysium around the regenerated muscle fibers containing centrally located nuclei, which are a hallmark of regeneration (Fig. 1, J and K). Although muscle regeneration following $BaCl_2$ injury is generally considered complete by 4 weeks after injury (*28*), altered ECM composition and elevated mechanical stiffness persist and do not return to preinjury levels by 28 days after injury.

In situ stiffening bioclick hydrogels recapitulate injury-mediated muscle stiffening

During regeneration, the elastic modulus of skeletal muscle changes markedly, possibly regulating cellular responses. To test this idea and control matrix mechanics independent of in vivo cytokine signaling (*2*), we developed hydrogels formed via a copper-free click reaction (SPAAC) between azides and activated cyclooctynes (i.e., *DBCO*), which can further undergo an in situ stiffening through a secondary photopolymerization of unreacted alkyne species to model ECM stiffening (Fig. 2A) (*14*). The mechanism involves a radical mediated photocrosslinking between unreacted DBCO groups, as the reaction can be inhibited with radical scavengers (fig. S1). We synthesized dynamic, stiffening networks using different stoichiometric ratios of DBCO groups (e.g., 2 to 4 equivalent with respect to $-N_3$ groups) to prepare hydrogels with initial Young's moduli ranging from $E' = 2$ to 16 kPa to a final photostiffened modulus of $E' = 32$ kPa (Fig. 2, B and C), spanning the range of moduli measured from in vivo muscle after injury. Network formulations further off-stoichiometry elevate the concentration of free alkynes and allowed us to achieve a larger difference in stiffness after secondary photocrosslinking. Using light as the initiator allows complete spatiotemporal control and the ability to fine-tune the extent of stiffening as a multistaged stiffening process (Fig. 2D).

MuSC proliferation and motility increase with substrate stiffness

To optimize our assays and minimize variability of primary cultured MuSC responses, we cultured C2C12 cells (a myoblast cell line derived from MuSCs) on SPAAC hydrogels with a 4:1 DBCO:N_3 stoichiometric ratio ($E' = 2$ kPa) and stiffened them to $E' = 32$ kPa by exposure to light (Fig. 2). To promote attachment, we incorporated a fibronectin-mimetic peptide sequence (N_3-KRGDS; 1 mM) within the network. C2C12 cells maintained myogenic transcription factor expression on $E' = 2$- and 32-kPa SPAAC hydrogels, as almost 100% of C2C12 cells were $Pax7^+/MyoD^+$ after 3 days in culture (Fig. 3, A and B). EdU was added for 2 hours before fixation to compare the number of cells synthesizing DNA across different hydrogel stiffnesses ($E' = 2$, 4, 12, and 32 kPa). Consistent with our observations for MuSCs in injured muscle, C2C12 cells proliferated more on $E' = 32$-kPa hydrogels (56% EdU^+) than when cultured on $E' = 2$-kPa hydrogels (42% EdU^+) (Fig. 3, C and D). When hydrogels were photostiffened from $E' = 2$ kPa to $E' = 24$ kPa 1 day after seeding, C2C12 cells increased DNA synthesis by 48 hours after stiffening to a level that was indistinguishable from C2C12 cells cultured continuously on $E' = 32$-kPa hydrogels (Fig. 3D). Since C2C12 cells are capable of dynamic increases in DNA synthesis as substrate elasticity changes, we predict that MuSCs are similarly capable of responding to dynamic stiffness changes occurring during muscle regeneration, providing mechanical regulation of cell division.

Activated MuSCs initiate migration along the ECM surrounding the injured myofiber (*3*). Since MuSCs remain activated along with the increased ECM stiffness after injury, we asked whether these mechanical properties would enhance motility of C2C12 cells. Single C2C12 cells were spatially tracked in real time over the course of 12 hours on different hydrogel stiffnesses (Fig. 3E). The mean velocity of C2C12 cells on 32-kPa hydrogels (29.4 μm/hour) and 12-kPa hydrogels (31.2 μm/hour) was higher compared to cells migrating on $E' = 2$-kPa hydrogels (24.6 μm/hour) (Fig. 3F). As increases in substrate stiffness led to higher cell motility and speed, we posit that substrate mechanics regulate and coordinate MuSC injury response during muscle regeneration.

The physical properties of muscle ECM are virtually impossible to control in vivo, making it challenging to study the influence of microenvironmental mechanics on primary MuSCs, while recapitulating the asymmetric niche between the sarcolemma of the myofiber and ECM (*29*). However, embedding myofibers with their resident MuSCs into hydrogels allows control of the external stiffness while preserving MuSC-myofiber interactions. To track location of MuSC progeny, we isolated myofibers from an EDL muscle of a $Pax7^{CreERT}$; ROSA26-lox-stop-$lox^{nls\text{-}tdTomato}$ mouse where recombination selectively labels $Pax7^+$ MuSCs with a nuclear localized tdTomato (Tom^+MuSC) (Fig. 4A). When Tom^+MuSCs on their associated myofibers were encapsulated in Matrigel (*30*), we observed extensive MuSC movement and a 16-fold increase in MuSC numbers over 3 days (Fig. 4B). In contrast, MuSC division was limited on myofibers encapsulated in a matching stiffness SPAAC hydrogel ($E' = 300$ Pa) (*31*), modified

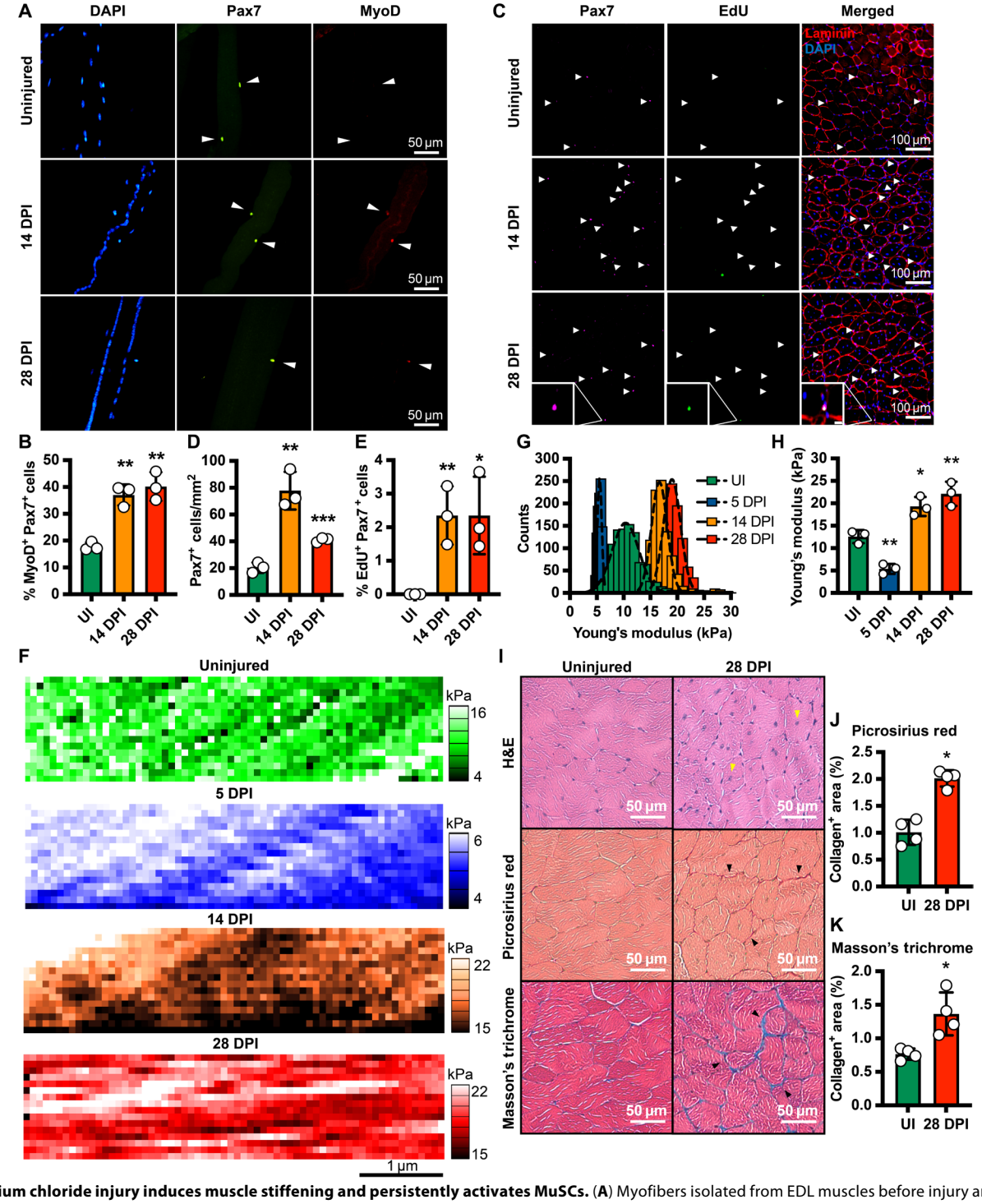

Fig. 1. Barium chloride injury induces muscle stiffening and persistently activates MuSCs. (**A**) Myofibers isolated from EDL muscles before injury and at 14 and 28 days after injury (DPI). MuSCs are immunoreactive for Pax7 and for MyoD upon activation. Nuclei are 4′,6-diamidino-2-phenylindole–positive ($DAPI^+$), and white arrowheads mark $Pax7^+$ MuSCs. (**B**) Quantification of the percentage of $MyoD^+$ expressing MuSCs. UI, uninjured. (**C**) TA muscle sections were assayed for EdU incorporation following 24-hour EdU pulse before harvest. Immunoreactivity to Pax7 identifies MuSCs, and laminin immunoreactivity demarcates the myofiber basement membrane; nuclei are detected by DAPI staining. White arrowheads identify EdU^- MuSCs, with EdU^+ MuSCs in the insert. Scale bars, 10 μm. Quantification of density (**D**) and percentage of EdU^+ (**E**) of $Pax7^+$ MuSCs at 14 and 28 days after injury. (**F**) Spatial Young's modulus maps of TA muscles measured by AFM. (**G**) Gaussian fits (dashed lines) of the frequency of the stiffness measurements and (**H**) their average values per muscle after injury. $n = 3$ biological replicates with three modulus maps per replicate. (**I**) TA muscle sections were stained with hematoxylin and eosin (H&E), Picrosirius red, and Masson's trichrome to identify collagen and the ECM. Yellow arrowheads mark examples of centrally located nuclei in regenerated myofibers, and black arrowheads mark increased collagen deposition. $n = 4$ biological replicates. The $collagen^+$ areas were quantified by Picrosirius (**J**) and Masson's trichrome staining (**K**). Unless otherwise noted, $n = 3$ biological replicates. For MuSC quantification, >50 MuSCs scored per replicate. Error bars represent the SD, and $^*P < 0.05$, $^{**}P < 0.01$, and $^{***}P < 0.001$ in a one-way analysis of variance (ANOVA) test compared to uninjured controls.

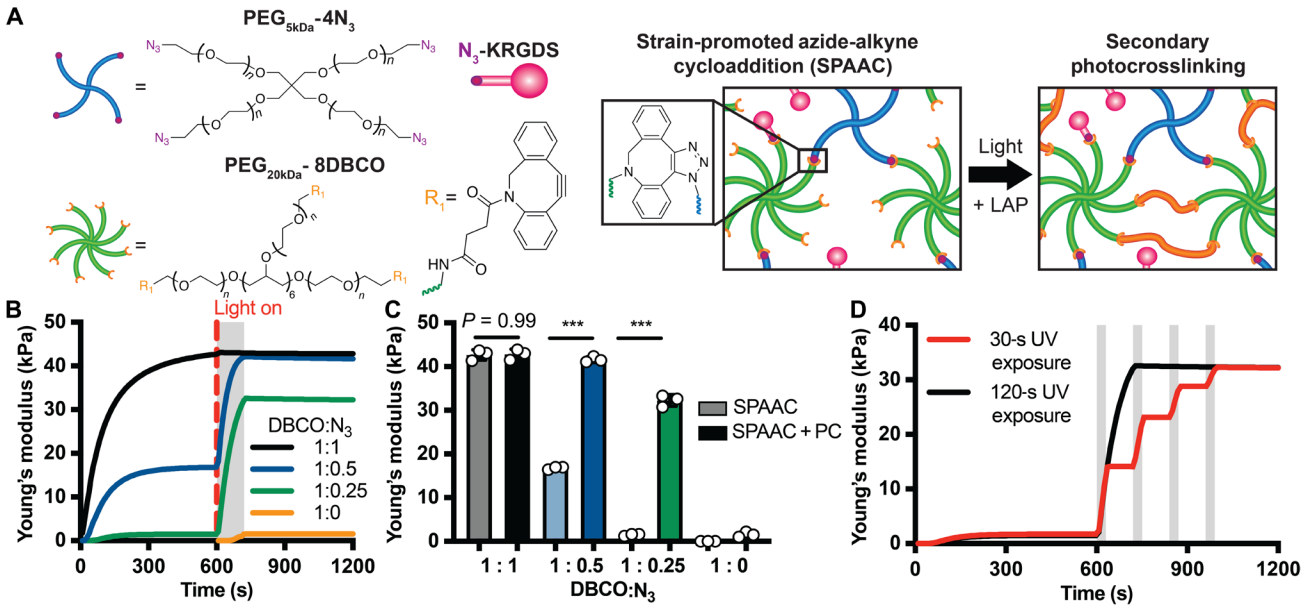

Fig. 2. Secondary photostiffening of SPAAC hydrogels to model muscle stiffening. (**A**) Schematic representation of hydrogel formation and the photocrosslinking reaction. Hydrogels are formed through a SPAAC reaction between cyclooctyne (PEG-DBCO)– and azide (PEG-N_3)–functionalized macromers, and the peptide N_3-KRGDS (1 mM) is incorporated to promote cell adhesion. Networks formed with an excess of DBCO functionalities can be further stiffened upon cytocompatible light irradiation in the presence of a photoinitiator (LAP). (**B**) Rheological traces of network evolution for different stoichiometric ratios of —DBCO and —N_3 functional groups. SPAAC network evolution is monitored for 600 s, followed by light exposure (365 nm, 10 mW/cm^2, 120 s; shaded region) to induce secondary photocrosslinking of pendant DBCO functionalities. (**C**) Quantification of Young's modulus for hydrogels with different DBCO to —N_3 stoichiometries before (striped) and after photocrosslinking (solid). $n = 3$ independent measurements, the plot displays the means ± SD, and ***$P < 0.001$ in a two-tailed Student's t test. (**D**) Stepwise network stiffening performed through consecutive 30-s light exposures, demonstrating tunability of the magnitude of stiffening entirely with light irradiation.

with azide-functionalized adhesive ligands derived from fibronectin (N_3-KRGDS; 1 mM) and laminin (N_3-IKVAV; 1 mM) to promote MuSC-matrix interactions (Fig. 4C and fig. S2). While Matrigel contains a complex milieu of growth factors, our synthetically defined SPAAC hydrogels better maintain MuSC quiescence, similar to that in uninjured muscle and without the need for mitogen activated kinase inhibitors to prevent activation (*9*). Under all hydrogel conditions, MuSCs remain viable as evidenced by continuous tdTomato expression. We increased the SPAAC hydrogel stiffness (E' = 300, 1000, 2400, and 4600 Pa) encapsulating the myofibers and observed a positive correlation between MuSC proliferation and hydrogel stiffness (Fig. 4, B and C). As the stiffness increases, MuSC division increases while maintaining myofiber interactions, directly demonstrating that primary MuSCs transduce the physical microenvironment into behavioral changes.

Yes-associated protein 1 and WW domain–containing transcription regulator 1 mediate mechanosensitive behavior of MuSCs

The transcriptional coactivators YAP (yes-associated protein 1) and TAZ [WW domain–containing transcription regulator 1 (WWTR1)] are mechanosensors that localize to the nucleus in response to increasing stiffness, promoting MuSC activation, subsequent cell proliferation, and stem cell differentiation (*32*–*37*). Increasing substrate moduli from E' = 2 to 32 kPa gradually increased YAP and TAZ nuclear localization in C2C12 cells (Fig. 5, A and B). In situ photostiffening from E' = 4 to 32 kPa after 24 hours of culture increased nuclear localization of YAP and TAZ, which did not occur when C2C12 cells were exposed to light or photoinitiator alone (Fig. 5C). Thus, YAP and TAZ subcellular localization is directly regulated by substrate stiffness in C2C12 cells, and the response time is approximately 24 hours or less.

YAP and TAZ nuclear localization may be responsible for stiffness-driven C2C12 proliferation, as YAP and TAZ translocation from the cytoplasm to the nucleus is mechanosensitive. To test this, we first inhibited YAP and TAZ nuclear import with verteporfin, a small-molecule inhibitor of YAP and TAZ, which up-regulates 14-3-3σ to sequester YAP in the cytoplasm and disrupts interactions with TEA domain transcription factors (TEADs) (*38*). After 24 hours of verteporfin supplementation (5 μM) on E' = 32-kPa hydrogels, YAP and TAZ nuclear localization declined by 20% (Fig. 5, D and E). Verteporfin concomitantly decreased C2C12 cell proliferation on E' = 32-kPa substrates to levels observed on E' = 4-kPa hydrogels (Fig. 5F), suggesting that YAP and TAZ signaling transduces mechanosensitive C2C12 cell proliferation.

Using a combination of short hairpin RNAs targeted to YAP and small-interfering RNA (siRNA) directed at TAZ, we assessed the individual roles of each protein on C2C12 responses (Fig. 5, G and H). ANKRD1 (ankyrin repeat domain 1) expression, an endogenous downstream target of YAP and TAZ (*39*), is elevated upon YAP loss but virtually eliminated upon TAZ knockdown or knockdown of both YAP and TAZ (Fig. 5G). Similarly, C2C12 cell proliferation is unaffected by YAP loss, but proliferation is inhibited by TAZ knockdown and by knockdown of both YAP and TAZ on E' = 32-kPa hydrogels (Fig. 5, I and J). YAP and TAZ transduce mechanosensitive proliferation synergistically, as removal of both proteins reduces the number of EdU$^+$ C2C12 cells (9.6% EdU$^+$) compared to TAZ removal (21% EdU$^+$). Thus, mechanical stimuli promote subcellular localization of YAP and TAZ, where these paralogs mediate proliferative responses, which are partially dominated by TAZ.

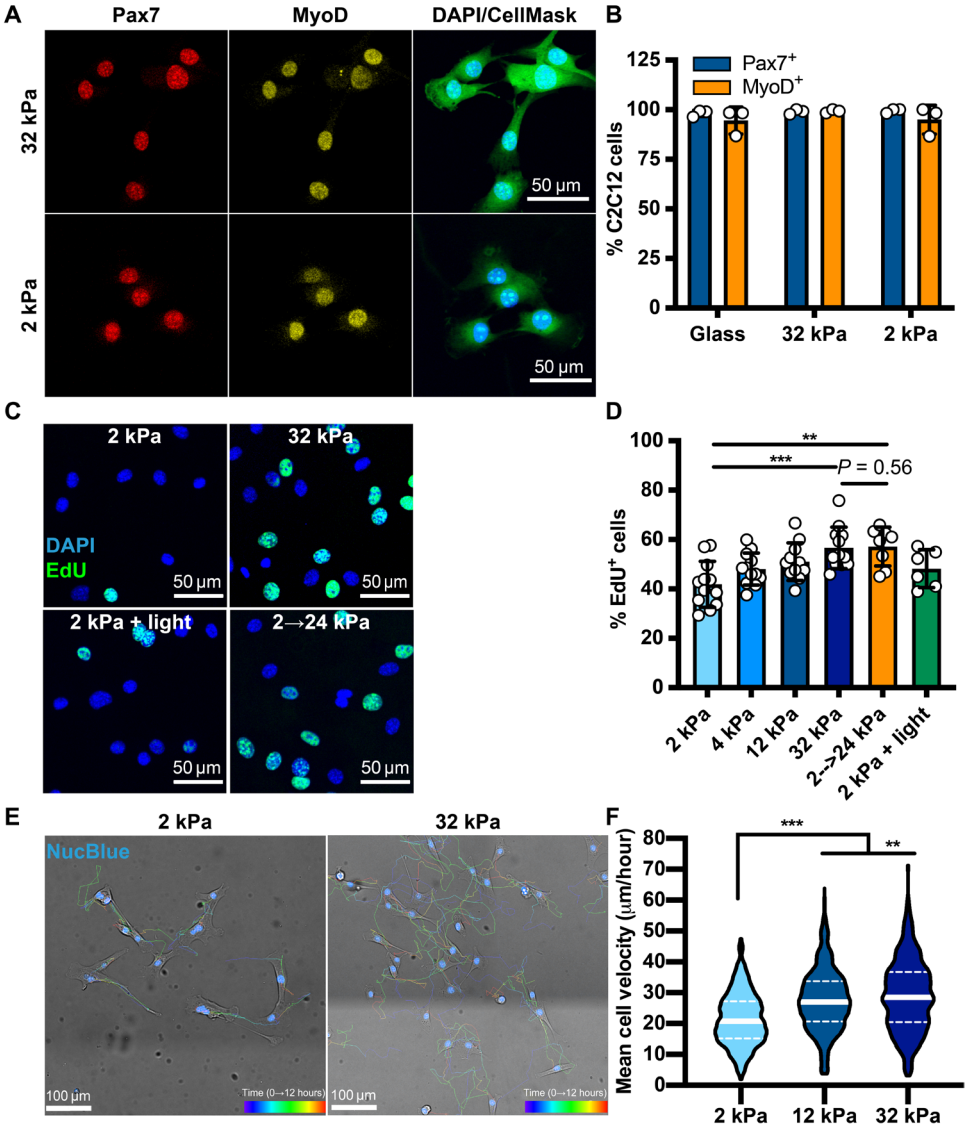

Fig. 3. C2C12 cell proliferation increases in response to dynamic stiffening substrates. (**A** and **B**) C2C12 cells cultured for 3 days on $E' = 2$- and 32-kPa SPAAC hydrogels retained Pax7 and MyoD expression. (**C**) Representative confocal images EdU incorporation in C2C12 cells after 2-hour EdU incubation. (**D**) EdU$^+$ cells were quantified as a function of substrate moduli between $E' = 2$ to 32 kPa before and after photostiffening. $n > 5$ biological replicates with >100 cells analyzed per replicate. (**E**) C2C12 cells were tracked in real time with NucBlue staining using Imaris software. Images were acquired every 15 min over 12 hours. (**F**) Violin plots of the average C2C12 migration velocity for 12 hours of tracking. Solid lines indicate the mean, and dashed lines mark the 25th and 75th quartiles. $n > 6$ with >180 cells counted per hydrogel. For (B) and (D), plots display the means ± SD, and $^{**}P < 0.01$ and $^{***}P < 0.001$ in a two-way ANOVA test.

Since matrix stiffness influences C2C12 cell behavior, we predict that MuSCs will similarly respond to changes in hydrogel stiffness. Similar to C2C12 cells, YAP and TAZ accumulate in the MuSC nucleus on stiffer substrates (Fig. 6A) and translocate directly to the MuSC nucleus after dynamic photostiffening (Fig. 6B). Accompanying elevated nuclear YAP and TAZ, transcripts for the target ANKRD1 are induced when cultured on E' = 32-kPa hydrogels (Fig. 6C). Consistent with the increase in YAP/TAZ nuclear localization, dynamic photostiffening increased the percentage of cycling MuSCs to that in static E' = 32-kPa hydrogels (Fig. 6, D and E). Thus, MuSCs sense and respond to dynamic changes in the substate stiffness by increasing steady-state YAP/TAZ nuclear localization and promoting a mechanosensitive proliferative response.

YAP and TAZ knockout decreases MuSC proliferation in postinjury, stiff muscle

To unequivocally demonstrate a requirement for YAP and TAZ in stiffness-dependent proliferation, we constructed MuSC conditional YAP and TAZ double knockouts by breeding Pax7^{CreERT} mice with YAP$^{flox/flox}$;TAZ$^{flox/flox}$ (dKO) mice (*40*). MuSCs from dKO mice cultured on E' = 2- and 32-kPa hydrogels for 48 hours in the presence or absence of tamoxifen reveal that YAP and TAZ ablation blocks substrate-dependent increases in proliferation in MuSCs (Fig. 6, F and G). Since injured skeletal muscle 28 days after injury is twofold stiffer than uninjured skeletal muscle (Fig. 1), we asked whether elevated MuSC proliferation detected in postinjured muscle is YAP/TAZ dependent. MuSC proliferation in vivo was assayed

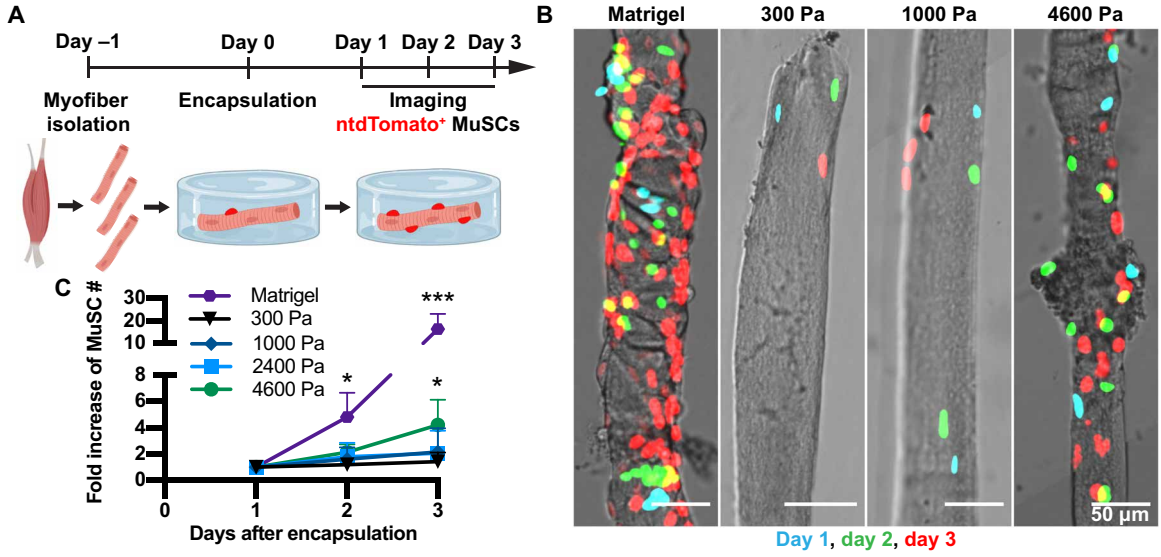

Fig. 4. Stiffness induces MuSC proliferation on encapsulated myofibers. (**A**) Myofibers from Pax7^{CreERT};ROSA26-stop-lox-stop$^{NLS\text{-}tdTOM}$ mice were isolated from an EDL muscle and cultured floating in media supplemented with 4-hydroxytamoxifen for 1 day to induce nuclear MuSC tdTomato expression (Tom$^+$MuSCs). Myofibers were encapsulated after 1 day of culture in either Matrigel or SPAAC hydrogels with stiffness values ranging between $E' = 300$ and 4600 Pa. Myofibers were imaged on three consecutive days. (**B**) Representative images of the encapsulated myofibers where Tom$^+$MuSCs are pseudo-colored on the basis of the imaging day and overlaid with the day 3 brightfield images. (**C**) Data are plotted for MuSCs cultured in Matrigel compared to stiffness-controlled SPAAC hydrogels ($E' = 300$ to 4600 Pa). $n > 6$ myofibers analyzed from three independent experiments, means ± SD, and $^*P < 0.05$ and $^{***}P < 0.001$ in a two-way ANOVA test comparing the means of other conditions to $E' = 300$-Pa SPAAC hydrogels.

following YAP and TAZ knockout at 14 days after injury and EdU incorporation between 21 and 28 days after injury (7 days) before tissue collection (Fig. 6H). In control mice, the numbers of MuSCs (Pax7$^+$; Fig. 6I) and their proliferation (EdU$^+$; Fig. 6J) increased in injured compared to contralateral (uninjured) muscles. In contrast, the YAP/TAZ knockout reverted the overall numbers of Pax7$^+$ cells and the numbers of proliferating Pax7$^+$ cells in injured muscle to amounts found in contralateral TA muscles. Furthermore, reduced MuSC numbers and reacquisition of quiescence in YAP/TAZ dKO MuSCs prevented myofiber hypertrophy that typically occurs upon muscle injury (Fig. 6K). Overall, these results imply that persistent exposure of MuSCs to stiffer postinjury microenvironment contributes to their unexpectedly activated and cycling state through YAP and TAZ signaling (Fig. 7).

DISCUSSION

Mechanical and chemical stresses acquired during muscle contraction require maintenance and repair by the endogenous stem cell population. Whether the MuSCs sense transient mechanical stresses during muscle contraction or the longer-term changes in elasticity that accompany injury or aging remains largely unknown. During muscle regeneration, longer-term changes in elasticity occur where muscle softens immediately following injury, then stiffens, and unexpectedly remains persistently stiff beyond completion of functional and morphological regeneration. Coinciding with muscle stiffening at 14 and 28 days following injury, MuSCs remain activated and proliferative compared to uninjured muscle, which questions whether these changes are partly caused by prolonged exposure to elevated stiffness, accompanying chemical signals or both. We first used dynamically stiffening hydrogels to determine that hydrogel stiffness induces proliferation, enhances motility, and localizes YAP/TAZ to the cell nucleus. YAP and TAZ persistently activate MuSCs upon exposure to elevated stiffness, as YAP and TAZ knockout after 14 days after injury reverted MuSC proliferation and muscle hypertrophy to uninjured levels.

Upon injury, skeletal muscle loses stiffness and is at least twofold softer than uninjured muscle by 5 days after injury. MuSCs are activated following injury and proliferate reaching their peak numbers by ~4 days after injury (*41*). Although muscle stiffness is low ($E' = 5$ kPa) due to the degradation of injured tissue, YAP and TAZ levels are elevated in MuSCs (*35*), as YAP is required to initiate MuSC activation and proliferation (*10*). The primary regulators of MuSC proliferation within the first 5 days after injury are likely secreted factors and possibly cell-cell interactions. For example, release of myofiber-bound Wnt (*10*) likely contributes to YAP and TAZ activation in MuSCs. The massive influx of immune cells and proliferation of fibroblasts elevates cytokines and increases ECM deposition (*41*, *42*). Thus, chemical signals likely override any effects of mechanical stimuli during rapid MuSC expansion, required to replenish the myonuclei. A combination of chemical and mechanical signals dictates MuSC behavior and is likely dependent on complex interactions with the surrounding microenvironment. In support of this, we observed extensive expansion of MuSCs embedded in Matrigel compared to an equivalent elasticity in an inert hydrogel.

Once myofibers have been repaired or remade and the majority of myonuclei produced, MuSC proliferation decreases markedly from ~7 to 14 days after injury, when morphological regeneration is complete. We observed that 10% of MuSCs continue proliferating between 21 and 28 days after injury, unexpectedly failing to reacquire quiescence. The regenerated muscle is significantly stiffer and remains elevated ($E' = 19$ to 22 kPa) compared to uninjured muscle ($E' = 12$ kPa) as a result of extensive collagen deposition. MuSCs in a defined environment respond to increased stiffness with elevated

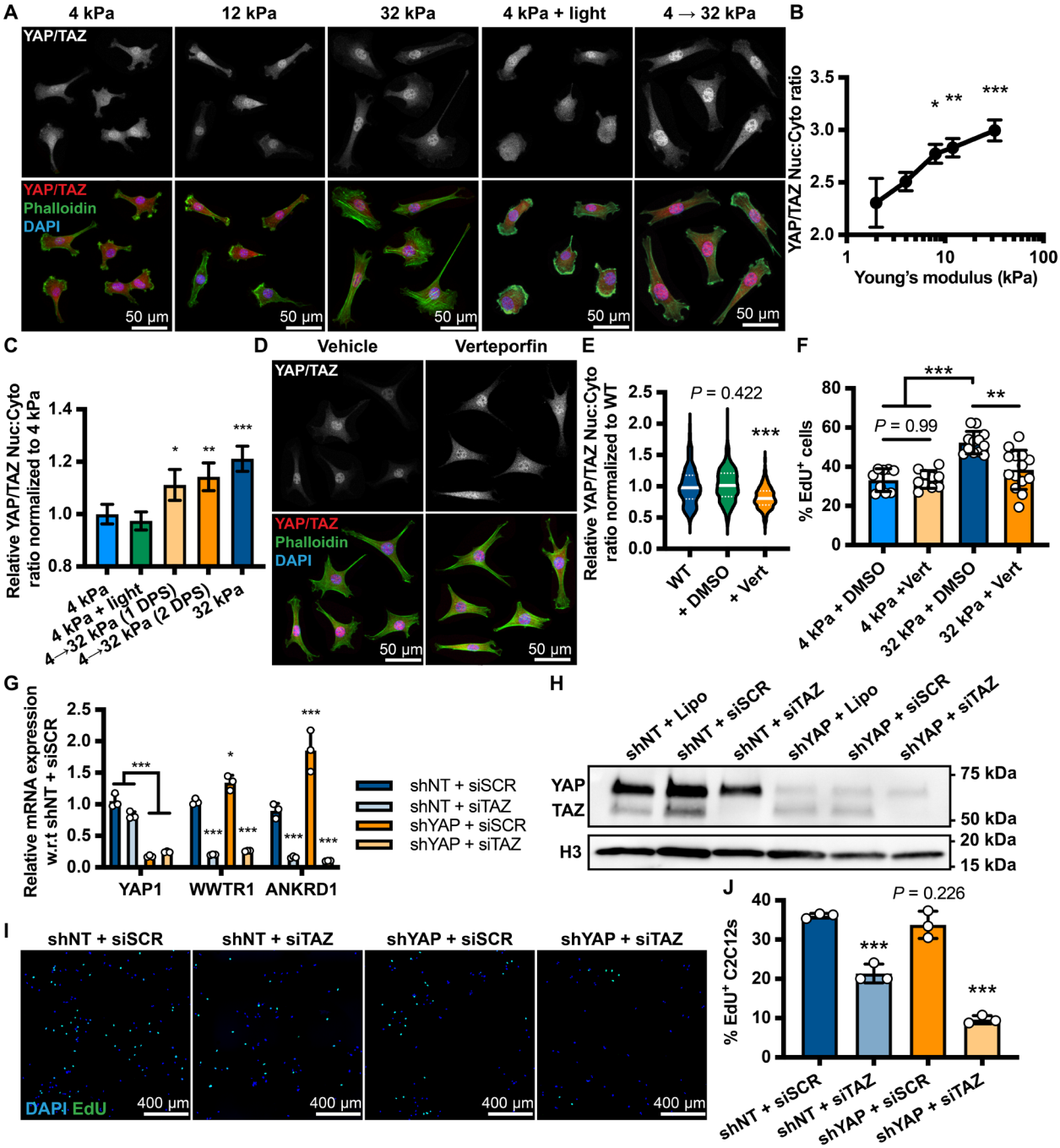

Fig. 5. YAP and TAZ mediate mechanosensitive C2C12 behavior. (**A**) Representative images of C2C12 cells cultured for 3 days on different stiffness hydrogels assayed for immunoreactivity to YAP and TAZ. Nuclear and cytoplasmic borders are demarcated by DAPI and phalloidin staining, respectively. (**B**) YAP/TAZ nuclear-to-cytoplasmic (Nuc:Cyto) ratio quantified as a function of substrate stiffness. Error bars represent 95% confidence intervals (CIs). (**C**) YAP/TAZ Nuc:Cyto ratio quantified upon in situ photostiffening and assayed at 1 and 2 days after stiffening (DPS). Error bars represent 95% CI. (**D**) Representative images of C2C12s cells treated with 5 μM verteporfin or vehicle control [dimethyl sulfoxide (DMSO)] for 24 hours. Verteporfin decreased YAP/TAZ Nuc:Cyto ratio in C2C12 cells. (**E**) Normalized YAP/TAZ Nuc:Cyto ratio of C2C12 cells with or without verteporfin treatment. (**F**) Quantification of EdU incorporation in C2C12 cells after 24 hours of 5 μM verteporfin treatment beginning on day 2 of culture. (**G**) Quantification of the mRNA expression and (**H**) protein levels of YAP and TAZ 48 hours after knockdown in C2C12 cells. YAP was knocked down with a short hairpin RNA (shRNA), and TAZ was knocked down with a siRNA. Each were compared to respective scrambled control vectors. shNT, non-targeted shRNA; siSCR, scrambled siRNA; w.r.t., with respect to. (**I**) Representative images for a 2-hour EdU incorporation after YAP and/or TAZ knockdown of C2C12 cells on 32-kPa hydrogels and their quantification (**J**). Unless noted elsewhere, $n > 3$ per experiment and >100 cells per hydrogel were quantified, means ± SD, and $^{*}P < 0.05$, $^{**}P < 0.01$, and $^{***}P < 0.001$ in a two-way ANOVA test.

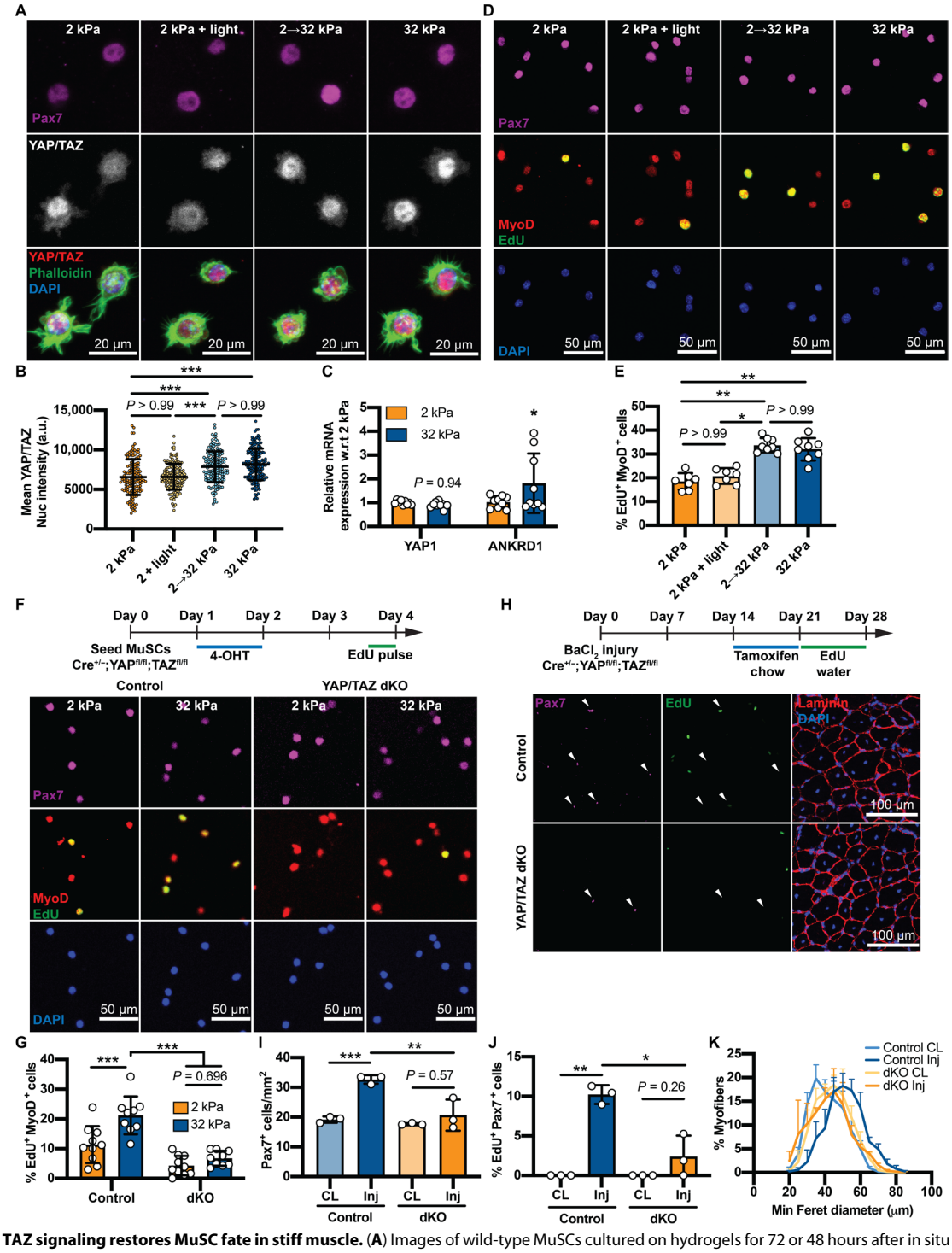

Fig. 6. YAP and TAZ signaling restores MuSC fate in stiff muscle. (**A**) Images of wild-type MuSCs cultured on hydrogels for 72 or 48 hours after in situ stiffening. MuSCs were identified by Pax7 immunoreactivity, assessed for subcellular YAP/TAZ localization with phalloidin and DAPI demarcating the cytoplasm and nucleus, respectively. (**B**) YAP/TAZ mean nuclear intensity was quantified on static and dynamically stiffened hydrogels. $n = 3$ with >15 cells scored per replicate. a.u., arbitrary units. (**C**) mRNA quantified by quantitative reverse transcription polymerase chain reaction (qRT-PCR) after 72 hours of culture. Images (**D**) and quantification (**E**) of EdU^+ MuSCs following an EdU treatment after 3 days after seeding or 2 days after in situ stiffening. (**F**) MuSCs from $Pax7^{CreERT}$;$YAP^{fl/fl}$;$TAZ^{fl/fl}$ mice were cultured on hydrogels. The medium was supplemented with 4-hydroxytamoxifen (4-OHT), and proliferation was assessed 48 hours later. Images of MuSCs immunoreactive for Pax7 and MyoD and assayed for EdU incorporation and quantification (**G**) of proliferating MuSCs. (**H**) Schematic for YAP/TAZ knockout and EdU treatment after injury in $YAP^{fl/fl}$;$TAZ^{fl/fl}$;$Pax7^{CreERT}$ (dKO) mice or $YAP^{fl/fl}$;$TAZ^{fl/fl}$;$Pax7^{+/+}$ (control) mice. Images of 28–day after injury TA muscle sections were assayed for EdU incorporation and immunoreactivity with laminin and Pax7 to identify MuSCs (white arrowheads). DAPI detected nuclei. Quantification of $Pax7^+$ (**I**) and EdU^+ (**J**) MuSCs from 28–day after injury or contralateral (CL) TA muscle sections. (K) Quantification of the myofiber minimum Feret diameter identified via laminin immunoreactivity. Unless noted elsewhere, $n = 3$ biological replicates. More than 50 MuSCs and >250 myofibers scored per replicate. Graphs display means ± SD, and $^*P < 0.05$, $^{**}P < 0.01$, and $^{***}P < 0.001$ in a one-way ANOVA test.

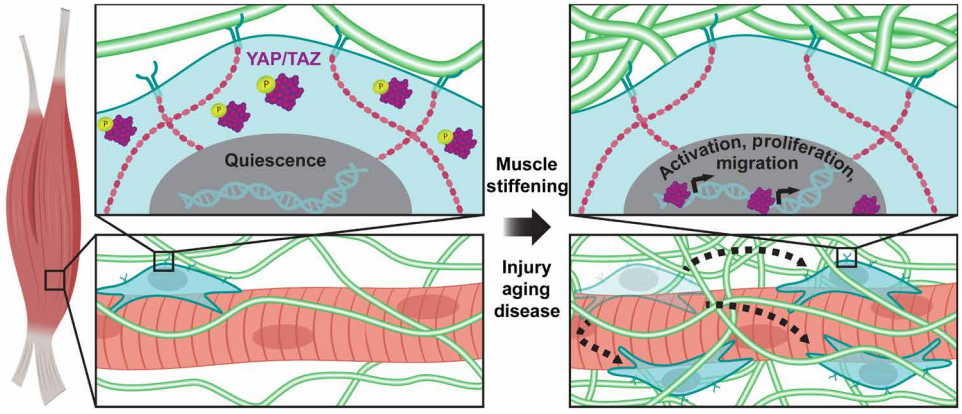

Fig. 7. Muscle stiffening induces mechanosensitive behavior through YAP and TAZ localization. A model for persistent injury-mediated mechanical stiffening of skeletal muscle promoting MuSC activation and proliferation. YAP and TAZ localization transduces the mechanical signals into proliferative MuSCs and enhances their migration.

proliferation, likely mediated by YAP and TAZ, which are well-established mechanosensors. YAP and TAZ activity is regulated by cytoskeletal tension (*39*), ligand density (*43*), and ECM composition (*44*), such that alternative ECM substrates, including fibronectin, induce different magnitudes of YAP and TAZ localization in C2C12 cells (*45*). Knockdown of YAP and TAZ in C2C12 cells or MuSCs abrogates stiffness-mediated proliferation, demonstrating that YAP and TAZ transduce the mechanical signals into cellular responses. However, YAP and TAZ are not functionally equivalent, as TAZ partially compensates for YAP loss and YAP knockdown is insufficient to eliminate stiffness-dependent proliferation or decrease gene expression of ANKRD1. Although we demonstrated that stiffness induces ANKRD1 expression, exogenous overexpression of constitutively activated YAP and TAZ does not alter ANKRD1 expression in MuSCs (*36*), identifying the complexities in interpreting YAP and TAZ function that are likely dependent on the cells, their substrate, and the culture environment. The gene dosage effects we observed for YAP and TAZ responses may explain why removal of either YAP or TAZ only marginally affects muscle regeneration (*36*).

If the elevated stiffness in injured skeletal muscle at 14 and 28 days after injury is responsible for increased YAP and TAZ that transduce the mechanical stimuli into cellular responses, then YAP and TAZ removal should revert MuSC behavior to that observed in uninjured skeletal muscle. Knocking out both YAP and TAZ at 14 days after injury restores MuSC quiescence. However, we noted that myofiber size was reduced compared to regenerated wild-type muscle, which may affect regenerated muscle function. Elevated muscle stiffness likely persists beyond 28 days; even 90 days after $BaCl_2$ injections, collagen levels remain high compared to uninjured muscle (*28*). The elevated stiffness and persistent MuSC proliferation responsible for myofiber hypertrophy may be necessary for restoring contractile strength following an injury. However, long-term exposure of MuSCs to elevated stiffness may be detrimental, gradually depleting the MuSC pool and exhausting the regenerative potential over long periods of time that occur in progressive myopathies and during aging. Whether these long-term changes can be modeled in hydrogel cultures is unclear, but incorporating ECM peptides mimics that stimulate ECM transitions from laminin to collagen after muscle injury (*29*) or during aging (*46*), may allow assessment of MuSC sensitivity to ECM switches.

Manipulation of hydrogel properties using innovative on-demand photostiffening SPAAC hydrogels offering precise mechanical control permitted us to establish that matrix stiffness directly promotes MuSC proliferation and enhances migration. Furthermore, we dynamically manipulated these hydrogels to demonstrate that YAP and TAZ are not functionally redundant. Last, we tested and confirmed the results of hydrogel cultures by in vivo knockout of YAP and TAZ, identifying that elevated stiffness in injured muscle promotes MuSC proliferation and myofiber hypertrophy. A persistent but gradual increase in muscle elasticity may contribute to regenerative impairment of skeletal muscle in progressive myopathies and during muscle aging.

MATERIALS AND METHODS

Mice

All mice were bred and housed according to National Institutes of Health (NIH) guidelines for the ethical treatment of animals in a pathogen-free facility at the University of Colorado at Boulder. All animal protocols and procedures were approved by the University of Colorado Institutional Animal Care and Use Committee, and the conducted studies complied with all ethical regulations. Wild-type mice were C57BL/6 J (the Jackson laboratory, stock no. 000664). Crossing ROSA26-lox-stop-lox$^{\text{nls-tdTomato}}$ mice (the Jackson laboratory, stock no, 025106) into the Pax7$^{\text{CreERT}}$ mice (*41*) generated the Pax7$^{\text{CreERT}}$;ROSA26-lox-stop-lox$^{\text{nls-tdTomato}}$ mice. For YAP/TAZ knockout, Pax7$^{\text{CreERT}}$ mice were crossed into the YAP1$^{\text{tm1Hmc}}$; WWTR1$^{\text{tm1Hmc}}$ mice (the Jackson laboratory, stock no. 030532). For litters of unknown genotype, tissue samples were collected at weaning and sent to Transnetyx for automated genotyping. Uninjured control mice were age- and sex-matched, and sample sizes were set at $n = 3$ unless otherwise noted.

Animal procedures

For chemical injuries, mice at 3 to 6 months old were first anesthetized with isoflurane, and then 50 μl of 1.2% $BaCl_2$ was injected into the left TA muscle. The injured and contralateral TA muscles were collected at the indicated time points. For EdU labeling of

proliferating MuSCs, EdU (0.5 mg/ml) (Carbosynth) with 1% glucose in water was provided before tissue collection and mice consumed ad libitum. To activate Cre^{ERT} in vivo for YAP/TAZ knockout, mice were fed a diet containing tamoxifen (250 mg/kg; Envigo) for 7 days.

Mechanical characterization of muscle tissue

AFM was performed on an Asylum Research Cypher AFM (Oxford Instruments, Santa Barbara, CA) to measure spatial variations in the mechanical properties of uninjured and injured tissue samples. The tissue sections were fixed to 18-mm glass coverslips via epoxy and then submerged in phosphate-buffered saline (PBS) at 25°C using the droplet cantilever holder and stage. Triangular SiN cantilevers with sharp Si tips (SNL-10, Bruker AFM Probes) were used both to minimize the interaction volume between measurements (nominal radius $R \approx 2$ nm) and to use a tip with a near-conical shape (nominal half-angle $\alpha \approx 22°$). The spring constant k_c of each cantilever was measured with the thermal fluctuation method (*47*); the resulting values for k_c ranged from 0.112 to 0.148 N/m with uncertainties of ≈0.002 N/m based on multiple measurements, in good agreement with the nominal value of 0.12 N/m from the manufacturer. Young's modulus maps were then generated by conducting force spectroscopy at each point in a 64 by 16 grid over a 5 μm by 1.25 μm area (≈80-nm pixel size). The force-displacement (*F*-*d*) measurements included both a loading and unloading curve; only the loading curves were considered here, as adhesive contributions were negligible, thereby simplifying the subsequent analyses. The *F*-*d* curves were converted to force-deformation (*F*-δ) data by subtracting out the cantilever deflection via the relationship $\delta = d - F/k_c$. Each *F*-δ curve was fit to an analytical model for a rigid conical tip in contact with an elastic half-space (*48*), $F = (2/\pi)(E/1\text{-}\nu^2)(\tan\alpha)\delta^2$, where the Poisson's ratio ν is assumed to be 0.5 as in previous work (*7*, *49*, *50*) and the Young's modulus *E* is the sole fitting parameter. Histograms of all *E* from the displayed maps were plotted, and the average values and SDs from measurements on three different samples were reported.

Histology and immunohistochemistry of tissues

To analyze the structural properties of muscle, TA muscles were dissected, fixed for 2 hours with 4% paraformaldehyde (PFA) on ice and transferred to 30% sucrose at 4°C overnight. The muscle was mounted in O.C.T. compound (Tissue-Tek), cryosectioned into 10-μm sections with a cryostat (Leica), and stored at −80°C until histological staining. Sections were stained with hematoxylin and eosin, Masson's trichrome, and Picrosirius red staining. For immunohistochemistry, tissue sections were postfixed with 4% PFA for 8 min at room temperature (RT) and washed three times for 5 min in PBS. For heat-induced epitope retrieval, which is required for Pax7 antibody staining, postfixed slides were placed in citrate buffer (pH 6.0) and subjected to 6 min of high pressure cooking (Cuisinart model CPC-600). Then, tissue sections were permeabilized with 0.25% Triton X-100 (Sigma-Aldrich) in PBS containing 3% bovine serum albumin (BSA; Sigma-Aldrich) for 45 min at RT. For EdU detection, the Click-iT EdU Alexa Fluor 488 detection kit (Molecular Probes) was used according to the manufacturer's protocols. For immunohistochemical staining, samples were incubated with primary antibody at 4°C overnight, washed three times in PBS, and then incubated with a secondary antibody in 3% BSA at RT for 1 hour. Primary and secondary antibodies were mouse anti-Pax7 (Developmental Studies Hybridoma Bank; 1:1000), rabbit anti-laminin (Sigma-Aldrich; 1:200), and Alexa Fluor 488, Alexa Fluor 555, and Alexa Fluor 647 (Molecular Probes; 1:750). Sections were incubated with 4′,6-diamidino-2-phenylindole (DAPI) (1 μg/ml) for 10 min at RT and then mounted in Mowiol supplemented with 1,4-diazabicyclo[2.2.2]octane (DABCO) (Sigma-Aldrich) as an antifade agent.

Myofiber isolation and immunocytochemistry staining

For myofiber isolation, the EDL muscles were dissected, placed into collagenase (400 U/ml) (Worthington) at 37°C for 1.5 hours with shaking, and then placed into Ham's F-12C (Gibco) supplemented with 15% horse serum (Gibco) to inactivate the collagenase. Individual EDL myofibers were separated and isolated using a flame-polished glass pipet. For immunocytochemistry, the myofibers were immediately fixed in 4% PFA for 10 min and stored in PBS for immunocytochemistry. Myofibers were permeabilized with 0.25% Triton X-100 in PBS containing 3% BSA (Sigma-Aldrich) for 45 min at RT and incubated with primary antibody at 4°C overnight, followed by incubation with secondary antibodies at RT for 1 hour. The primary and secondary antibodies were mouse anti-Pax7 (Developmental Studies Hybridoma Bank; 1:1000), rabbit anti-MyoD (Santa Cruz Biotechnology; 1:250), and Alexa Fluor 488, Alexa Fluor 555, and Alexa Fluor 647 (Molecular Probes; 1:750). Following immunolabeling, myofibers were incubated with DAPI (1 μg/ml) for 10 min at RT and then mounted in Mowiol supplemented with DABCO (Sigma-Aldrich) as an antifade agent.

Hydrogel preparation

Eight-arm PEG-DBCO (20,000 g/mol) (*14*), four-arm PEG-DBCO (20,000 g/mol) (*14*), four-arm PEG-N_3 (5000 g/mol) (*15*), and N_3-GRGDS (*51*) were synthesized as previously described. To form SPAAC hydrogels, PEG-DBCO (5%, w/v) and N_3-KRGDS (1 mM) were prereacted for 5 min on ice in PBS. Then, PEG-N_3 was added at different concentrations to obtain DBCO/N_3 stoichiometries ranging from 4 to 1 together with excess PBS. The mixture was vortexed, and the 15 μl of the gel solutions were sandwiched between a sigma-coated (Sigma-Aldrich) glass cover slide and an azide-functionalized 12-mm glass coverslip, which is prepared using previously established protocols (*52*). The gelation was allowed to continue for 5 min at RT to obtain 2D SPAAC hydrogels. To obtain $E' = 32$-kPa hydrogels, 2 mM lithium phenyl-2,4,6 trimethylbenzoylphosphinate (LAP) was also added to the hydrogel solution, and the hydrogels were irradiated with light (365 nm, 10 mW/cm^2, 2 min) following the initial gelation.

Rheology

Rheological traces were collected in situ on shear rheometer (TA Instruments Discovery HR3) equipped with a parallel plate geometry and a light curing accessory. Frequency and amplitude sweeps were performed to ensure that measurement was within the linear viscoelastic range [1% strain, 1 rad/s (radians/second)]. SPAAC network formation was monitored for 600 s before light irradiation (365 nm, 10 mW/cm^2, 120 s), from an ultraviolet (UV) lamp (OmniCure S2000). To prevent sample dehydration during the experiment, samples were sealed with a thin ring of mineral oil (Sigma-Aldrich).

C2C12 cell culture

C2C12 cells were obtained from American Type Culture Collection, and all studies were conducted with cells under passage 16. C2C12 cells were grown in growth medium [high-glucose Dulbecco's modified

Eagle's medium (DMEM) supplemented with 20% (v/v) fetal bovine serum (FBS; Life Technologies), 1% (v/v) sodium pyruvate (Sigma-Aldrich), 1% (v/v) L-glutamine (Gibco), 1% (v/v) penicillin-streptomycin (Gibco), and amphotericin B (0.5 μg/ml; Gibco)]. Cultures were maintained at 5% CO_2 and 37°C. For experiments, C2C12 cells were collected by a 5 min trypsinization (Gibco) and seeded at a density of 1000 cells/cm^2 on prepared hydrogel substrates.

C2C12 cell immunocytochemistry

Samples for immunostaining were fixed in 4% PFA at RT for 15 min. After removing fixative, samples were washed three times with PBS for 10 min and stored in PBS at 4°C before staining. Samples were permeabilized using 0.1% Triton X-100 in PBS for 1 hour and blocked with 5% BSA for 1 hour at RT. Anti-YAP/TAZ (Santa Cruz Biotechnology, SC-101199; 1:250), anti-Pax7 (Developmental Studies Hybridoma Bank; 1:1000), anti-laminin (Sigma-Aldrich, L9393; 1:200), and anti-MyoD (Santa Cruz Biotechnology, SC-760; 1:200) were used as primary antibodies and incubated for overnight at 4°C in 5% BSA. After three washes in PBST (0.05 weight % Tween 20 in PBS) for 10 min, Alexa Fluor 488–, Alexa Fluor 555–, and Alexa Fluor 647–conjugated secondary antibodies (Invitrogen; 1:400) and DAPI (Sigma-Aldrich; 1 μg/ml) were added in 5% BSA. After 1 hour, samples were washed three times with PBS for 10 min. After immunocytochemistry, all samples were kept at 4°C before imaging.

C2C12 cell proliferation assays

To quantify proliferation of C2C12 cells as a function of substrate stiffness, a 2-hour 10 μM EdU (Thermo Fisher Scientific) pulse was carried out 72 hours after seeding. The samples were subsequently rinsed in 5% BSA in PBS twice and then permeabilized with 0.5% Triton X-100 for 1 hour. After two more washes with 5% BSA, samples were incubated with the Click-iT reaction cocktail prepared using the Click-iT EdU Alexa Fluor 488 kit (Thermo Fisher Scientific) for 30 min. The reaction cocktail was removed, and cells were washed with 5% BSA. Secondary immunostaining was performed as above.

C2C12 cell migration assays

To quantify the motility, C2C12s were fluorescently tracked after 48 hours of culture on different hydrogel stiffnesses. Before imaging, NucBlue (Thermo Fisher Scientific) was incubated at 2 drops/ml of media for 30 min to fluorescently label the nucleus. C2C12 cells were then cultured in phenol-free growth media and imaged continuously for 12 to 14 hours. Images were acquired in every 15 min on a Nikon Ti-E microscope equipped with an Okolab environmental chamber. Using Imaris software (Bitplane), C2C12 migration was quantified for all cells tracked for greater than 4 hours. The mean cell velocity was defined as the average of the instantaneous velocity calculated at each time point for each track.

Myofiber encapsulation

Myofibers were isolated from an EDL of a Pax7^{CreERT};ROSA26-lox-stop-lox$^{nls\text{-}tdTomato}$ mouse as described above. After halting the collagenase digestion, individual myofibers were manually picked and cultured in suspension in Ham's F-12C (Gibco) supplemented with 15% horse serum (Gibco), 1% (v/v) penicillin-streptomycin (Gibco), 50 nM fibroblast growth factor 2, and 1 μM 4-hydroxytamoxifen (Sigma-Aldrich) in noncoated sterile petri dishes for 24 hours at 5% CO_2 and 37°C. To embed myofibers, approximately 20 myofibers were placed into a glass bottom 96-well plate (Cellvis) and allowed to settle for 10 min in the incubator. After careful removal of the excess media, 50 μl of the Matrigel (Corning) or hydrogel solution was added dropwise to resuspend and fully encapsulate the myofibers with the ECM substrates. The gel solutions polymerized for 10 min in the incubator, and then fresh medium was added to each well. For the SPAAC hydrogels, the PEG-DBCO [four-arm, 20,000 g/mol, 5% (w/v)] was prereacted with N_3-GRGDS (1 mM) and N_3-IKVAV (1 mM) in PBS. Immediately after media removal from the myofibers, PEG-N_3 (four-arm, 5000 g/mol) was added at different concentrations to obtain DBCO/N_3 stoichiometries and stiffnesses (fig. S2). Embedded myofibers were maintained in the incubator and imaged every 24 hours for three consecutive days.

MuSC isolation and culture

To isolate primary MuSCs, hindlimb muscles were dissected out of the mouse, mechanically diced into a puree, and enzymatically digested in collagenase (4000 U/ml) in Ham's F-12C media (Gibco) for 1 hour at 37°C, vigorously shaking every 10 min. Collagenase was then inactivated by 15% horse serum (Gibco). The muscle digest was then passed through 100-, 70-, and 40-μm filters (Thermo Fisher Scientific) to isolate single cells. The flow-through was the centrifuged at 200 rcf (relative centrifugal force) for 5 min and resuspended in Ham's F-12C media with MyoCult Expansion Supplement (STEMCELL Technologies). MuSCs were selectively enriched by exclusion to adhering to plastic for 1 hour and then replated onto collagen coated plastic for one passage at 5% CO_2 and 37°C. For culture on hydrogels, MuSCs were collected via a 3-min trypsinization (Gibco) and seeded at a density of 7500 cells/cm^2 on prepared hydrogel substrates in Ham's F-12C with MyoCult Expansion Supplement. Hydrogels with 1 mM N_3-GRGDS were additionally surface coated with Matrigel (Corning; 1:100 dilution in DMEM) for 30 min at 37°C to promote MuSC attachment. For dynamic photostiffening, 2 mM LAP was supplemented for 30 min before light exposure (365 nm, 10 mW/cm^2, 2 min).

YAP and TAZ knockdown in C2C12 cells

For YAP knockdown, lentiviral transduction particles [Mission shRNA (short hairpin RNA)] encoding short hairpin sequence for YAP (shYAP; TRCN0000238436) were purchased from Functional Genomics Facility of University of Colorado Cancer Center. Control lentiviral transduction particles were purchased from Sigma-Aldrich (SHC002V). For the generation of shYAP and shNT-C2C12 cell lines, C2C12 cells were seeded on tissue culture plastic with a density of 4000 cells/cm^2 at day 0. After 16 hours, lentiviral transduction particles with a multiplicity of infection ranging from 10 to 100 were delivered together with polybrene (6 μg/ml). Starting from D3, cells that incorporate shRNA constructs were selected using puromycin (2.5 μg/ml) for 7 to 12 days. Surviving colonies reaching subconfluency were passaged twice during puromycin selection to prevent premature differentiation of C2C12 cells. After puromycin selection, three to six selected colonies were expanded, and the successful knockdown of YAP was determined using quantitative reverse transcription polymerase chain reaction (qRT-PCR) and Western blotting. For TAZ knockdown, predesigned Stealth siRNAs for WWTR1 (Invitrogen, MSS251009) or a controlled RNA (Invitrogen) that does not target any mammalian gene were used (table S1). C2C12 cells were seeded at a density of 1500 cells/cm^2. After 24 hours, siRNAs (at 25 pmol/cm^2) were mixed with Lipofectamine 2000

(Thermo Fisher Scientific) with a concentration of 0.875 μl/cm^2, and the transfection was allowed to continue for 16 hours. After 16 hours, cells were supplemented with the fresh growth media, and the extent of TAZ knockdown and the C2C12 cell proliferation were quantified after 48 hours after transfection.

mRNA analysis with qRT-PCR

Total RNA was collected and purified using a RNeasy mini kit (QIAGEN) per the manufacturer's protocol. The RNA concentration and quality were assessed with a ND-1000 NanoDrop spectrophotometer. For qRT-PCR, complementary DNA was synthesized with the iScript Reverse Transcription Supermix Kit (Bio-Rad) and the Eppendorf Mastercycler. Relative mRNA expression levels were measured using SYBR Green reagents (Bio-Rad) with an iCycler machine (Bio-Rad) and normalized to the glyceraldehyde-3-phosphate dehydrogenase housekeeping gene. Three technical replicates were carried out per condition, and custom primers (Invitrogen) are presented in table S1.

Protein analysis with Western blots

Chemiluminescence Western blot techniques were used to assess the YAP/TAZ protein after knockdown. Total protein was collected by lysing C2C12s for 10 min on ice with radioimmunoprecipitation assay buffer (Thermo Fisher Scientific) supplemented with 1:100 halt phosphatase and protease inhibitor (Thermo Fisher Scientific). Protein concentrations were determined with micro BCA kit (Bio-Rad), and 5 to 10 μg of protein were loaded into each lane. The protein lysate was diluted with Laemmli SDS buffer (Alfa Aesar) and heated for 5 min to 95°C. The protein extracts and Precision Plus Protein Ladder (Bio-Rad) were run on Mini-PROTEAN TGX 4 to 12% precast protein gels (Bio-Rad) for approximately 1 hour at 120 V. The gels were transferred in buffer of 25 μM tris-base (Sigma-Aldrich), 175 μM glycine (Sigma-Aldrich), and 10% methanol (Sigma-Aldrich) for 90 min at 0.4 A and 130 V at 4°C using standard Western blotting protocols onto 0.45-μm nitrocellulose blotting membranes (GE Healthcare). Blots were blocked in TBST [tris-buffered saline (TBS) + 0.05% Tween 20] with 5% skim milk powder for 1 hour at RT and subsequently incubated overnight with primary YAP/TAZ antibody (Santa Cruz Biotechnology, SC-101199; 1:2000) and histone H3 (Abcam, ab1791; 1:5000) diluted in blocking solution (TBST + 5% BSA) at 4°C. Membranes were incubated with a secondary horseradish peroxidase–conjugated antibody (Jackson ImmunoResearch, anti-mouse or anti-rabbit; 1:5000) for 1 hour at RT. The chemiluminescence signal was detected using Pierce enhanced chemiluminescence plus solution (Thermo Fisher Scientific) and an ImageQuant LAS 4000 detector.

Imaging and image analysis

Images of immunolabeled samples were collected on a Zeiss LSM710 scanning confocal microscope with a 20× numerical aperture (N.A.) 1.0 objective. tdTomato$^+$ MuSCs on embedded myofibers were imaged with an environmentally controlled CellVoyager CV1000 Confocal Scanner System (Olympus) using a 10× N.A. 0.4 objective. For all YAP/TAZ studies, samples were imaged on the PerkinElmer Operetta using the confocal setting with a 20× objective. YAP nuclear-to-cytoplasmic (Nuc:Cyto) ratio and cell area were analyzed using Harmony software (PerkinElmer). Nuclear and cytoplasmic areas were defined using DAPI and Alexa Fluor 488 phalloidin staining, respectively. The inherent autofluorescence of the background in 555-nm channel (YAP/TAZ) was subtracted from the analysis.

Statistical analysis

All statistical analyses were performed in Prism (GraphPad). To assess statistical significance, two-tailed, unpaired Student's t test, one-way analysis of variance (ANOVA), and two-way ANOVAs were performed, and $P < 0.05$ was considered significant. At least three different replicates were used per study. For YAP/TAZ studies, approximately 100 cells from each sample were analyzed, and three independent samples were analyzed per experimental condition ($n = 300$ cells total). First, a one-way ANOVA test was first carried out to determine whether sampling variability exists ($P < 0.05$). If it does not exist, then cells from these samples were pooled, and another one-way ANOVA test was carried out to determine statistical significances among different experimental conditions.

Graphical illustration

Some graphical images of muscles, myofibers, and hydrogels were created with BioRender.com.

SUPPLEMENTARY MATERIALS

Supplementary material for this article is available at http://advances.sciencemag.org/cgi/content/full/7/11/eabe4501/DC1

View/request a protocol for this paper from *Bio-protocol*.

REFERENCES AND NOTES

1. J. R. Sanes, The basement membrane/basal lamina of skeletal muscle. *J. Biol. Chem.* **278**, 12601–12604 (2003).
2. K. Thomas, A. J. Engler, G. A. Meyer, Extracellular matrix regulation in the muscle satellite cell niche. *Connect. Tissue Res.* **56**, 1–8 (2015).
3. M. T. Webster, U. Manor, J. Lippincott-Schwartz, C. M. Fan, Intravital imaging reveals ghost fibers as architectural units guiding myogenic progenitors during regeneration. *Cell Stem Cell* **18**, 243–252 (2016).
4. E. W. Li, O. C. McKee-Muir, P. M. Gilbert, Cellular biomechanics in skeletal muscle regeneration. *Curr. Top. Dev. Biol.* **126**, 125–176 (2018).
5. M. A. Green, R. Sinkus, S. C. Gandevia, R. D. Herbert, L. E. Bilston, Measuring changes in muscle stiffness after eccentric exercise using elastography. *NMR Biomed.* **25**, 852–858 (2012).
6. F. Trensz, F. Lucien, V. Couture, T. Söllrald, G. Drouin, A.-J. Rouleau, M. Grandbois, G. Lacraz, G. Grenier, Increased microenvironment stiffness in damaged myofibers promotes myogenic progenitor cell proliferation. *Skelet. Muscle.* **5**, 5 (2015).
7. A. J. Engler, M. A. Griffin, S. Sen, C. G. Bönnemann, H. L. Sweeney, D. E. Discher, Myotubes differentiate optimally on substrates with tissue-like stiffness: Pathological implications for soft or stiff microenvironments. *J. Cell Biol.* **166**, 877–887 (2004).
8. B. D. Cosgrove, P. M. Gilbert, E. Porpiglia, F. Mourkioti, S. P. Lee, S. Y. Corbel, M. E. Llewellyn, S. L. Delp, H. M. Blau, Rejuvenation of the muscle stem cell population restores strength to injured aged muscles. *Nat. Med.* **20**, 255–264 (2014).
9. M. Quarta, J. O. Brett, R. DiMarco, A. De Morree, S. C. Boutet, R. Chacon, M. C. Gibbons, V. A. Garcia, J. Su, J. B. Shrager, S. Heilshorn, T. A. Rando, An artificial niche preserves the quiescence of muscle stem cells and enhances their therapeutic efficacy. *Nat. Biotechnol.* **34**, 752–759 (2016).
10. S. Eliazer, J. M. Muncie, J. Christensen, X. Sun, R. S. D'Urso, V. M. Weaver, A. S. Brack, Wnt4 from the niche controls the mechano-properties and quiescent state of muscle stem cells. *Cell Stem Cell* **25**, 654–665.e4 (2019).
11. P. M. Gilbert, K. L. Havenstrite, K. E. G. Magnusson, A. Sacco, N. A. Leonardi, P. Kraft, N. K. Nguyen, S. Thrun, M. P. Lutolf, H. M. Blau, Substrate elasticity regulates skeletal muscle stem cell self-renewal in culture. *Science* **329**, 1078–1081 (2010).
12. W. M. Han, M. Mohiuddin, S. E. Anderson, A. J. García, Y. C. Jang, Co-delivery of Wnt7a and muscle stem cells using synthetic bioadhesive hydrogel enhances murine muscle regeneration and cell migration during engraftment. *Acta Biomater.* **94**, 243–252 (2019).
13. A. Bauer, L. Gu, B. Kwee, W. A. Li, M. Dellacherie, A. D. Celiz, D. J. Mooney, Hydrogel substrate stress-relaxation regulates the spreading and proliferation of mouse myoblasts. *Acta Biomater.* **62**, 82–90 (2017).
14. T. E. Brown, J. S. Silver, B. T. Worrell, I. A. Marozas, F. M. Yavitt, K. A. Günay, C. N. Bowman, K. S. Anseth, Secondary photocrosslinking of click hydrogels to probe

myoblast mechanotransduction in three dimensions. *J. Am. Chem. Soc.* **140**, 11585–11588 (2018).
15. C. A. DeForest, K. S. Anseth, Cytocompatible click-based hydrogels with dynamically tunable properties through orthogonal photoconjugation and photocleavage reactions. *Nat. Chem.* **3**, 925–931 (2011).
16. C.-H. Wong, S. C. Zimmerman, Orthogonality in organic, polymer, and supramolecular chemistry: From Merrifield to click chemistry. *Chem. Commun.* **49**, 1679–1695 (2013).
17. H.-Y. Liu, T. Greene, T.-Y. Lin, C. S. Dawes, M. Korc, C.-C. Lin, Enzyme-mediated stiffening hydrogels for probing activation of pancreatic stellate cells. *Acta Biomater.* **48**, 258–269 (2017).
18. S. Rammensee, M. S. Kang, K. Georgiou, S. Kumar, D. V. Schaffer, Dynamics of mechanosensitive neural stem cell differentiation. *Stem Cells* **35**, 497–506 (2017).
19. S. Khetan, J. A. Burdick, Patterning network structure to spatially control cellular remodeling and stem cell fate within 3-dimensional hydrogels. *Biomaterials* **31**, 8228–8234 (2010).
20. D. P. Nair, N. B. Cramer, J. C. Gaipa, M. K. McBride, E. M. Matherly, R. R. McLeod, R. Shandas, C. N. Bowman, Two-stage reactive polymer network forming systems. *Adv. Funct. Mater.* **22**, 1502–1510 (2012).
21. S. R. Caliari, M. Perepelyuk, B. D. Cosgrove, S. J. Tsai, G. Y. Lee, R. L. Mauck, R. G. Wells, J. A. Burdick, Stiffening hydrogels for investigating the dynamics of hepatic stellate cell mechanotransduction during myofibroblast activation. *Sci. Rep.* **6**, 21387 (2016).
22. M. P. Lutolf, J. A. Hubbell, Synthesis and physicochemical characterization of end-linked poly(ethylene glycol)-co-peptide hydrogels formed by Michael-type addition. *Biomacromolecules* **4**, 713–722 (2003).
23. K. A. Günay, T. L. Ceccato, J. S. Silver, K. L. Bannister, O. J. Bednarski, L. A. Leinwand, K. S. Anseth, PEG–Anthracene hydrogels as an on-demand stiffening matrix to study mechanobiology. *Angew. Chemie. Int. Ed.* **58**, 9912–9916 (2019).
24. M. Guvendiren, J. A. Burdick, Stiffening hydrogels to probe short- and long-term cellular responses to dynamic mechanics. *Nat. Commun.* **3**, 792 (2012).
25. B. Pawlikowski, C. Pulliam, N. D. Betta, G. Kardon, B. B. Olwin, Pervasive satellite cell contribution to uninjured adult muscle fibers. *Skelet. Muscle* **5**, 42 (2015).
26. A. de Morree, J. D. D. Klein, Q. Gan, J. Farup, A. Urtasun, A. Kanugovi, B. Bilen, C. T. J. Van Velthoven, M. Quarta, T. A. Rando, Alternative polyadenylation of Pax3 controls muscle stem cell fate and muscle function. *Science* **366**, 734–738 (2019).
27. N. C. Jones, K. J. Tyner, L. Nibarger, H. M. Stanley, D. D. W. Cornelison, Y. V. Fedorov, B. B. Olwin, The p38α/β MAPK functions as a molecular switch to activate the quiescent satellite cell. *J. Cell Biol.* **169**, 105–116 (2005).
28. D. Hardy, A. Besnard, M. Latil, G. Jouvion, D. Briand, C. Thépenier, Q. Pascal, A. Guguin, B. Gayraud-Morel, J. M. Cavaillon, S. Tajbakhsh, P. Rocheteau, F. Chrétien, Comparative study of injury models for studying muscle regeneration in mice. *PLOS ONE* **11**, e0147198 (2016).
29. H. Yin, F. Price, M. A. Rudnicki, Satellite cells and the muscle stem cell niche. *Physiol. Rev.* **93**, 23–67 (2013).
30. M. E. Danoviz, Z. Yablonka-Reuveni, Skeletal muscle satellite cells: Background and methods for isolation and analysis in a primary culture system. *Methods Mol. Biol.*, (2012).
31. S. S. Soofi, J. A. Last, S. J. Liliensiek, P. F. Nealey, C. J. Murphy, The elastic modulus of Matrigel™ as determined by atomic force microscopy. *J. Struct. Biol.* **167**, 216–219 (2009).
32. S. Piccolo, S. Dupont, M. Cordenonsi, The biology of YAP/TAZ: Hippo signaling and beyond. *Physiol. Rev.* **94**, 1287–1312 (2014).
33. C. Yang, M. W. Tibbitt, L. Basta, K. S. Anseth, Mechanical memory and dosing influence stem cell fate. *Nat. Mater.* **13**, 645–652 (2014).
34. M. Ohgushi, M. Minaguchi, Y. Sasai, Rho-signaling-directed YAP/TAZ activity underlies the long-term survival and expansion of human embryonic stem cells. *Cell Stem Cell* **17**, 448–461 (2015).
35. R. N. Judson, A. M. Tremblay, P. Knopp, R. B. White, R. Urcia, C. D. Bari, P. S. Zammit, F. D. Camargo, H. Wackerhage, The Hippo pathway member Yap plays a key role in influencing fate decisions in muscle satellite cells. *J. Cell Sci.* **125**, 6009–6019 (2012).
36. C. Sun, V. De Mello, A. Mohamed, H. P. Ortuste Quiroga, A. Garcia-Munoz, A. Al Bloshi, A. M. Tremblay, A. von Kriegsheim, E. Collie-Duguid, N. Vargesson, D. Matallanas, H. Wackerhage, P. S. Zammit, Common and distinctive functions of the hippo effectors Taz and Yap in skeletal muscle stem cell function. *Stem Cells* **35**, 1958–1972 (2017).
37. K. I. Watt, R. Judson, P. Medlow, K. Reid, T. B. Kurth, J. G. Burniston, A. Ratkevicius, C. De Bari, H. Wackerhage, Yap is a novel regulator of C2C12 myogenesis. *Biochem. Biophys. Res. Commun.* **393**, 619–624 (2010).
38. K. Brodowska, A. Al-Moujahed, A. Marmalidou, M. Meyer, zu Horste, J. Cichy, J. W. Miller, E. Gragoudas, D. G. Vavvas, The clinically used photosensitizer verteporfin (VP) inhibits YAP-TEAD and human retinoblastoma cell growth in vitro without light activation. *Exp. Eye Res.* **124**, 67–73 (2014).
39. S. Dupont, L. Morsut, M. Aragona, E. Enzo, S. Giulitti, M. Cordenonsi, F. Zanconato, J. Le Digabel, M. Forcato, S. Bicciato, N. Elvassore, S. Piccolo, Role of YAP/TAZ in mechanotransduction. *Nature* **474**, 179–183 (2011).
40. A. Reginensi, R. P. Scott, A. Gregorieff, M. Bagherie-Lachidan, C. Chung, D. S. Lim, T. Pawson, J. Wrana, H. McNeill, Yap- and Cdc42-dependent nephrogenesis and morphogenesis during mouse kidney development. *PLOS Genet.* **9**, e1003380 (2013).
41. M. M. Murphy, J. A. Lawson, S. J. Mathew, D. A. Hutcheson, G. Kardon, Satellite cells, connective tissue fibroblasts and their interactions are crucial for muscle regeneration. *J. Cell Sci.* **124**, e1 (2011).
42. W. Yang, P. Hu, Skeletal muscle regeneration is modulated by inflammation. *J. Orthop. Translat.* **13**, 25–32 (2018).
43. A. E. Stanton, X. Tong, S. Lee, F. Yang, Biochemical ligand density regulates yes-associated protein translocation in stem cells through cytoskeletal tension and integrins. *ACS Appl. Mater. Interfaces* **11**, 8849–8857 (2019).
44. A. E. Stanton, X. Tong, F. Yang, Extracellular matrix type modulates mechanotransduction of stem cells. *Acta Biomater.* **96**, 310–320 (2019).
45. W. J. Hadden, J. L. Young, A. W. Holle, M. L. McFetridge, D. Y. Kim, P. Wijesinghe, H. Taylor-Weiner, J. H. Wen, A. R. Lee, K. Bieback, B. N. Vo, D. D. Sampson, B. F. Kennedy, J. P. Spatz, A. J. Engler, Y. S. Cho, Stem cell migration and mechanotransduction on linear stiffness gradient hydrogels. *Proc. Natl. Acad. Sci. U.S.A.* **114**, 5647–5652 (2017).
46. H. M. Blau, B. D. Cosgrove, A. T. V. Ho, The central role of muscle stem cells in regenerative failure with aging. *Nat. Med.* **21**, 854–862 (2015).
47. J. L. Hutter, J. Bechhoefer, Calibration of atomic-force microscope tips. *Rev. Sci. Instrum.* **64**, 1868–1873 (1993).
48. I. N. Sneddon, The relation between load and penetration in the axisymmetric boussinesq problem for a punch of arbitrary profile. *Int. J. Eng. Sci.* **3**, 47–57 (1965).
49. A. M. Collinsworth, S. Zhang, W. E. Kraus, G. A. Truskey, Apparent elastic modulus and hysteresis of skeletal muscle cells throughout differentiation. *Am. J. Physiol. Cell Physiol.* **283**, C1219–C1227 (2002).
50. G. Lacraz, A. J. Rouleau, V. Couture, T. Söllrald, G. Drouin, N. Veillette, M. Grandbois, G. Grenier, Increased stiffness in aged skeletal muscle impairs muscle progenitor cell proliferative activity. *PLOS ONE* **10**, e0136217 (2015).
51. T. E. Brown, I. A. Marozas, K. S. Anseth, Amplified photodegradation of Cell-Laden hydrogels via an addition–fragmentation chain transfer reaction. *Adv. Mater.* **29**, 1605001 (2017).
52. B. J. Adzima, Y. Tao, C. J. Kloxin, C. A. DeForest, K. S. Anseth, C. N. Bowman, Spatial and temporal control of the alkyne-azide cycloaddition by photoinitiated Cu(II) reduction. *Nat. Chem.* **3**, 256–259 (2011).

Acknowledgments: For AFM measurements, certain commercial equipment, instruments, or materials are identified to specify the experimental procedure adequately. This identification is not intended to imply recommendation or endorsement by NIST, nor is it intended to imply that the materials or equipment identified is necessarily the best available for the purpose. For histological sections and staining, we appreciate the contribution to this research made by E. E. Smith, A. Quador, and J. Arnold of the University of Colorado Denver Tissue Biobanking and Histology Shared Resource, supported in part by the Cancer Center Support Grant (P30CA046934). Migration assays were performed and analyzed at the BioFrontiers Institute Advanced Light Microscopy Core supported by the Howard Hughes Medical Institute and NIH 1S10RR026680-01A1. Imaging encapsulated myofibers was accomplished in the Light Microscopy Facility, Porter at the University of Colorado Boulder. **Funding:** This work was supported by grants from the NIH (DE016523 and DK120921) to K.S.A. and NIH (AR049446 and AR070360) to B.B.O. **Author contributions:** K.S.A., B.B.O., J.S.S., K.A.G., A.A.C., T.O.V., T.E.B., and B.T.P. designed the studies, analyzed the data, and wrote the manuscript. F.W.D. performed and analyzed the AFM measurements. O.J.B., K.L.B., C.J.R., and A.G.M. performed bench work, data collection, and statistical analysis. **Competing interests:** B.O. is a member of the Scientific Advisory Board for Satellos Biosciences. All other authors declare that they have no competing interests. **Data and materials availability:** All data needed to evaluate the conclusions in the paper are present in the paper and/or the Supplementary Materials. Additional data related to this paper may be requested from the authors.

Submitted 21 August 2020
Accepted 27 January 2021
Published 12 March 2021
10.1126/sciadv.abe4501

Citation: J. S. Silver, K. A. Günay, A. A. Cutler, T. O. Vogler, T. E. Brown, B. T. Pawlikowski, O. J. Bednarski, K. L. Bannister, C. J. Rogowski, A. G. Mckay, F. W. DelRio, B. B. Olwin, K. S. Anseth, Injury-mediated stiffening persistently activates muscle stem cells through YAP and TAZ mechanotransduction. *Sci. Adv.* **7**, eabe4501 (2021).